

Monte Carlo AVO Analysis For Lithofacies Classification

Tapan Mukerji^{1*}, Scott Singleton², Marie Schneider³, Miguel Ascanio², and Richard Uden²

¹Stanford Rock Physics Laboratory, Stanford University

²Rock Solid Images

³Statoil

Summary

The objective of this work is to use AVO intercept and gradient, in conjunction with well-log petrophysics analysis, to discriminate and classify lithofacies in a shaly sand reservoir. Careful log and core analysis, and rock physics modeling was used to identify the important seismic litho-classes. Monte Carlo AVO simulations based on statistical rock physics was used to set up the class-conditioned probability distributions (pdfs) of intercept and gradient. The effect of thin-layer anisotropy on the probability distributions of AVO intercept and gradient was considered by simulating various realizations of sand-shale thin layers. Monte Carlo simulations, by taking into account distributions of values instead of single average values, help to avoid the flaw of averages. Monte Carlo simulations also give us confidence intervals and other measures of uncertainty. Computations using averages and average trends alone do not give any indication of the uncertainty due to the variability in the properties. The pdfs were then used to classify the seismic AVO intercept and gradient cubes to estimate the most-likely facies and obtain lithofacies probability cubes.

Introduction

The reservoir of interest is a deepwater Tertiary formation from the Norwegian Sea. A full suite of well logs and core data were available from one well. The well discovered oil in laminated, low permeability reservoir. Three of the log-derived curves are shown in Figure 1. The sandstones are very clay rich with average V_{shale} of 0.38. Figure 2 shows that the sands in general have a higher acoustic impedance than the shales, and a lower VP/VS ratio. Increase in oil saturation also reduces the VP/VS ratio, while the acoustic impedance of the oil sands are in between those of the shales and the wet sands. Careful petrophysical analysis indicated the presence of glauconite within the sands. At a fixed porosity, the presence of glauconite reduces P-wave velocity and impedance in quartz sandstones (Diaz et al., 2003). Rock physics modeling indicated that the unconsolidated sands model (Dvorkin and Nur, 1996) was appropriate for these sandstones at the well. Estimates of pore pressure based on a combination of formation pressure data (RCI tool) and mud weight measurements indicated the presence of overpressure in the formation. The overpressure effects were incorporated in modeling the pore fluid properties for fluid substitution. The fluid effect

is large because of the “soft” compressible rock frame properties. Core and log analysis helped to identify the basic seismic-scale lithostratigraphic elements as consisting of sand-mud alterations with thin sand beds ranging from less than 25cm to some beds about 100cm or more. Thin-bed anisotropy, using Backus averaging (Backus, 1962) has to be included when modeling the seismic signatures of the reservoir.

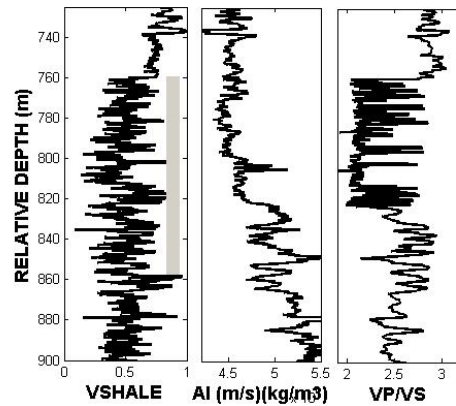


Figure 1: Logs around the zone of interest. The acoustic impedance (center) is computed from the P-wave sonic and density logs. The gray bar denotes the reservoir. Depths are not absolute depths.

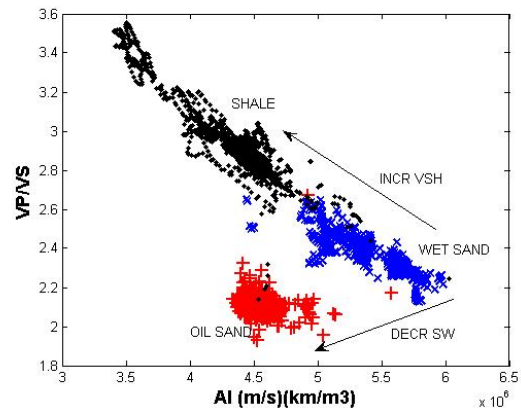


Figure 2: Rock physics template of acoustic impedance versus VP/VS ratio showing variation in the properties of different groups, and trends of saturation and shaliness.

Monte Carlo AVO and Lithofacies Classification

Methodology

We applied the statistical rock physics workflow as described in Mukerji et al., (2001) and Avseth et al., (2005). In brief the workflow consists of the following steps: 1) based on well log rock physics and core information, identify a discrete number of seismic lithofacies. Ultimately the seismic data volume will be mapped into these discrete lithofacies. Avseth (2000) defines seismic lithofacies by one of the following criteria: a) It has a distinct lithological/geological definition or b) It has distinct acoustical properties. For example, oil saturated sands and brine saturated sands are considered distinct seismic lithofacies since each of them may have a different elastic/seismic signature. 2) Derive multivariate probability distributions of seismic attributes using correlated Monte Carlo simulations with inputs based on the multivariate distributions of rock properties for each identified seismic lithofacies. The results from this step are the class-conditioned probabilities, $\text{Prob}(\text{seismic attributes} | \text{lithofacies})$. 3) Classify the seismic attributes extracted from the seismic data using a statistical classification scheme to get the posterior probabilities, $\text{Prob}(\text{lithofacies} | \text{seismic attribute})$ and generate the lithocube output.

Results

Figure 3 shows a scatter plot of Monte Carlo simulated values of intercept and gradient for shale/oil sand, shale/wet sand and shale/shale pairs. These points are used to estimate the bivariate pdfs of intercept and gradient for each class.

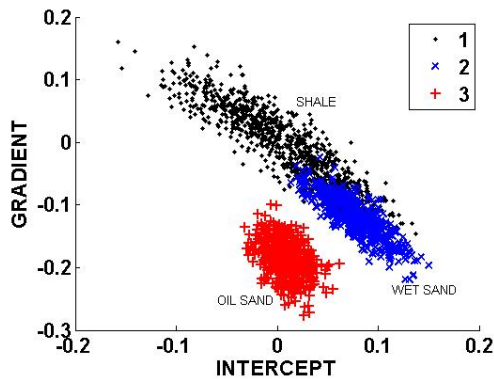


Figure 3: Monte-Carlo simulated values of intercept ($R(0)$) and gradient (G) plotted on a scatter plot color-coded by the facies type: 1=shale; 2=wet sand; 3=oil sand. Simulations based on well log rock properties.

As mentioned in the introduction, due to the laminated nature of the lithostratigraphic elements, it is necessary to incorporate the effect of thin-layer anisotropy on the seismic signatures.

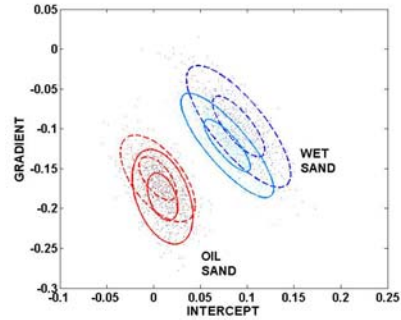


Figure 4: Effect of thin layer anisotropy on the pdfs of intercept and gradient. Contours with dashed curves are pdfs from isotropic Monte Carlo calculations, ignoring the thin layers. Solid curves are pdfs when thin layer anisotropy is incorporated. Because of the change in the pdfs, the classification decision boundary shifts. Samples that would have been classified as oil sand with the isotropic pdfs will now be classified as wet.

This was done in the Monte Carlo simulations by taking a Backus average of the sand properties with the reservoir shale properties, over a distribution of sand/shale proportions. Backus averaging gave a TIV (transversely isotropic, vertical symmetry axis) medium for the reservoir rock. The anisotropic Thomsen's parameters (ϵ, δ, γ) for the caprock were estimated from VSP data. The anisotropic intercept and gradient were computed using Thomsen's approximation (Thomsen, 1993) for the P-wave reflection coefficient for TIV media. The calculations were done for each Monte Carlo realization. Figure 4 compares the intercept-gradient pdfs from the anisotropic simulations versus the pdfs obtained ignoring thin-layer anisotropy (i.e. isotropic calculations, without Backus averaging). Thin-layer anisotropy shifts the pdfs, the effect depending on whether it is wet sand or oil sand. Consequently, the discrimination boundary between the classes also shifts. This may cause potential pitfalls in the classification. Samples that would have been classified as oil sand with the isotropic pdfs will now be classified as wet sand when thin layer effect is included.

The pdfs derived from the Monte Carlo simulations are used to classify the seismically derived intercept and gradient. The average misclassification error for the training pdfs was 9%. Before the classification can be done, the raw intercept and gradient values have to be scaled and calibrated to the derived pdfs. The calibration is done by re-scaling the global covariance of the raw data. The data are first transformed into their z-scores (zero mean, unit variance), and then the global covariance matrix is used to rescale the data. Figure 5 shows the data after calibration.

Monte Carlo AVO and Lithofacies Classification

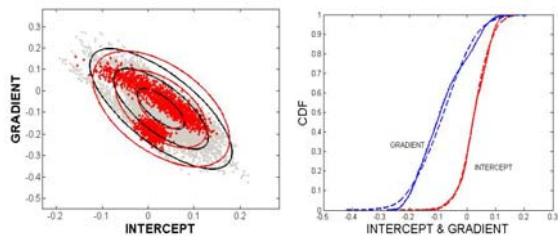


Figure 5: Left: Scatter plot and pdf contours of the Monte Carlo simulated intercept and gradient (red) and the seismically derived intercept and gradient (gray) after covariance based calibration. Right: Cumulative distributions of the Monte Carlo simulated (solid curves) intercept (red) and gradient (blue) and the seismic intercept and gradient (dashed curve) after calibration.

The calibrated data is then classified to get the lithocube and the posterior probabilities for each facies (Figure 6). The statistical classification was done using discriminant analysis (Hastie et al., 2001). The predicted lithofacies at the well location (Figure 6, center right) shows a good match to the two zones of oil sands that were interpreted from the well logs. Of course, this is not a strict validation as the well was used for the training data in the classification system. The probability cubes and lithocubes can be displayed in combination using color and transparency. Figure 7 (left) shows voxels classified as oil sands with color and opacity proportional to the probability of oil sand. Lower probabilities are transparent while higher probabilities are more opaque. Figure 7 (right) is an indicator display indicating predicted facies = oil sands and posterior probability of oil sand > 0.7. Another indicator that can be useful for interpretation is the second principal component of the data. Figure 8 shows the data transformed to the principal component coordinate axes. For this reservoir, strongly negative second principal component is indicative of oil sand. The cube of the second principal component with transparency proportional to the value highlights zones that might be interpreted as oil sands (compare Figures 9 and 7).

Conclusions

Lithofacies were classified use AVO intercept and gradient, in conjunction with well-log petrophysics analysis. Careful log and core analysis, and rock physics modeling was used to identify the important seismic litho-classes. Monte Carlo AVO simulations based on statistical rock physics was used to set up the class-conditioned probability distributions (pdfs) of intercept and gradient. The effect of thin-layer anisotropy on the probability distributions of AVO

intercept and gradient was considered by simulating various realizations of sand-shale thin layers. Ignoring thin-layer anisotropy may cause potential pitfalls in the classification. The pdfs were then used to classify the seismic AVO intercept and gradient cubes to estimate the most-likely facies and obtain lithofacies probability cubes. Various combination displays of the lithocube and probability cube were presented as an aid to interpretation.

Acknowledgments

We thank Statoil for the data and permission to present this work. We acknowledge the support of the LFP project and the Stanford Rock Physics Project (SRB) and its affiliates.

References

- Avseth, P., 2000, Combining rock physics and sedimentology for seismic reservoir characterization of North Sea turbidite system, Ph.D. dissertation, Stanford University.
- Avseth, P., Mukerji, T., and Mavko, G., 2005, *Quantitative Seismic Interpretation: Applying Rock Physics Tools to Reduce Interpretation Risk*, Cambridge University Press, 359pp.
- Backus, G. E., 1962, Long-wave elastic anisotropy produced by horizontal layering, *J. Geophys. Res.*, **67**, 4427-4420.
- Diaz, E., Prasad, M., Mavko, G. and Dvorkin, J., 2003, Effect of glauconite on the elastic properties, porosity, and permeability of reservoir rocks, *The Leading Edge*, **22**, 42-45
- Dvorkin, J., and Nur, A., 1996, Elasticity of high-porosity sandstones: Theory for two North Sea datasets, *Geophysics*, **61**, 1363-1370.
- Hastie, T., Tibshirani, R., and Freidman, J., 2001, *The Elements of Statistical Learning. Data Mining, Inference, and Prediction*, Springer-Verlag, New York, 533p.
- Mukerji, T., Avseth, P., Mavko, G., Takahashi, I., and Gonzalez, E., 2001, Statistical rock physics; combining rock physics, information theory, and geostatistics to reduce uncertainty in seismic reservoir characterization, *The Leading Edge*, **20**, 313-319
- Thomsen, L., 1993, Weak anisotropic reflections, in *Offset Dependent Reflectivity – Theory and Practice of AVO analysis*, Castagna, J. P., and Backus, M., eds., SEG, Tulsa.

Monte Carlo AVO and Lithofacies Classification

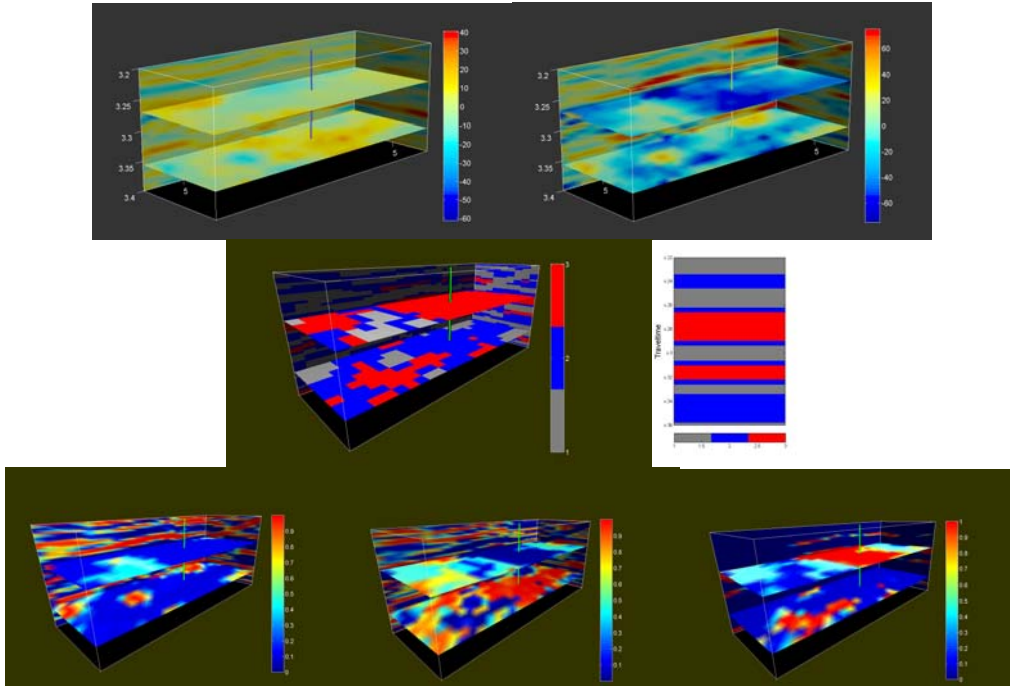


Figure 6: Seismic cubes of AVO intercept (top left) and gradient (top right) were used as inputs to the classification system to estimate the most-likely facies (center) and obtain three cubes of posterior probability for each facies (bottom). Center: color indicates facies with gray for shale, blue for wet sands and red for oil sands. Center left: The estimated lithocube. Center right: Predicted lithofacies at the well location. The probability cubes (bottom) are for shale, wet sand and oil sand respectively from left to right. Vertical line near center of cube indicates well.

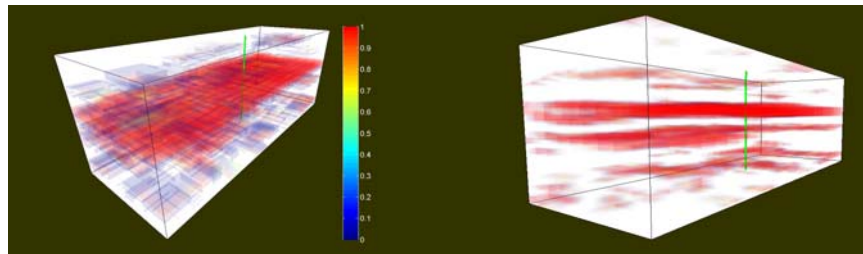


Figure 7: Left: Voxels classified as oil sands with color and opacity proportional to the probability of oil sand. Lower probabilities are more transparent. Right: Indicator display indicating predicted facies = oil sands and posterior probability of oil sand > 0.7

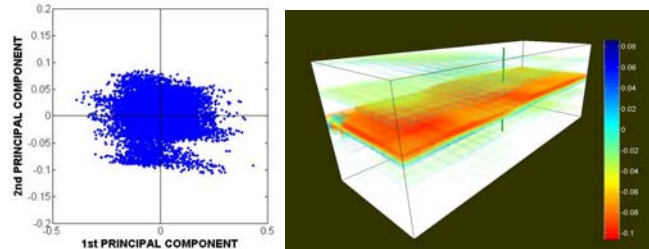


Figure 8: Left: Data transformed to the principal component coordinate axes. Right: Cube of the second principal component with transparency proportional to the value highlights zones that might be interpreted as oil sands (compare Figures 8 and 7).